Indian Journal of Radio & Space Physics
Vol. 15, October & December 1986, pp. 217-234

Ionospheric Modelling during the Past Decades

K RAWER
Albert – Ludwigs – Universität, D-7800 Freiburg, FRG

Starting with oversimplified models (e.g. reflecting mirror) geometrical optics in a parabolic layer achieved a satisfactory explanation of the most important phenomena in ionospheric hf-propagation. Later, more detailed descriptions of the electron density profile were developed, e.g. the International Reference Ionosphere. These are based on ground and space observations. The C.C.I.R. 'numerical maps' describing the world-wide behaviour of the peak data are rediscussed now. Sophisticated theoretical models based on aeronomic theory have been developed during the last 15 years. These need an enormous computing effort.

1. Introduction

The existence of a conducting layer in the atmosphere was first inferred from magnetic observations by Stewart[1] and Schuster[2], then from vlf-propagation results by Kennely[3] and Heaviside[4]. The very detection of an ionosphere might, however, be attributed to those radio amateurs who in 1921 realized almost lossless transatlantic communication via hf waves. Since that time, modelling of the ionosphere started mainly for sake of radio wave propagation. It was soon found that mirror-like reflection was unable to explain the occurrence of a skip distance. Refraction in a layer of upwards decreasing refractive index n was the solution. Figure 1, taken from S.K. Mitra's famous book[5] shows how each ray follows the refraction law:

$$n \cdot \sin \phi = \text{const} = 1 \cdot \sin i \quad (1)$$

ϕ being the angle against the vertical, i its value at the bottom of the layer. It appears that ray bending might be so strong that its direction becomes horizontal somewhere. This happens at a level where the reflection condition

$$n_r = \sin i \quad (2)$$

holds.

Since the refractive index of a plasma varies with the wave frequency (refraction being stronger at lower frequency), one may find at a given frequency that the steepest rays nowhere fulfill the reflection condition and therefore penetrate the layer. The first ray which is bent determines the radius of the skip zone (Fig. 2b). Going up with the frequency increases this zone (Fig. 2c) while going down decreases it. If the frequency is low enough, the reflection condition is satisfied even at vertical incidence: no skip zone appears (Fig. 2a). The first frequency, for which this happens to be true, is called critical frequency, f_c. Now, assuming a thin layer, the angle of incidence of the skip zone ray can be computed from simple geometry. Then, with the dependence of n on frequency and for a given distance d, one easily obtains a relation between the critical frequency f_c and that frequency f which has d for skip zone radius. Figure 3 shows the ratio f/f_c as function of skip distance d for diffe-

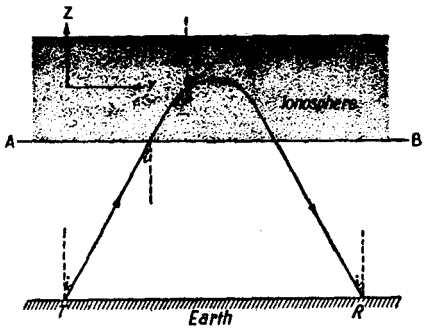

Fig.1 - Refraction (index decreasing upwards) in vertically stratified medium (after S K Mitra[5])

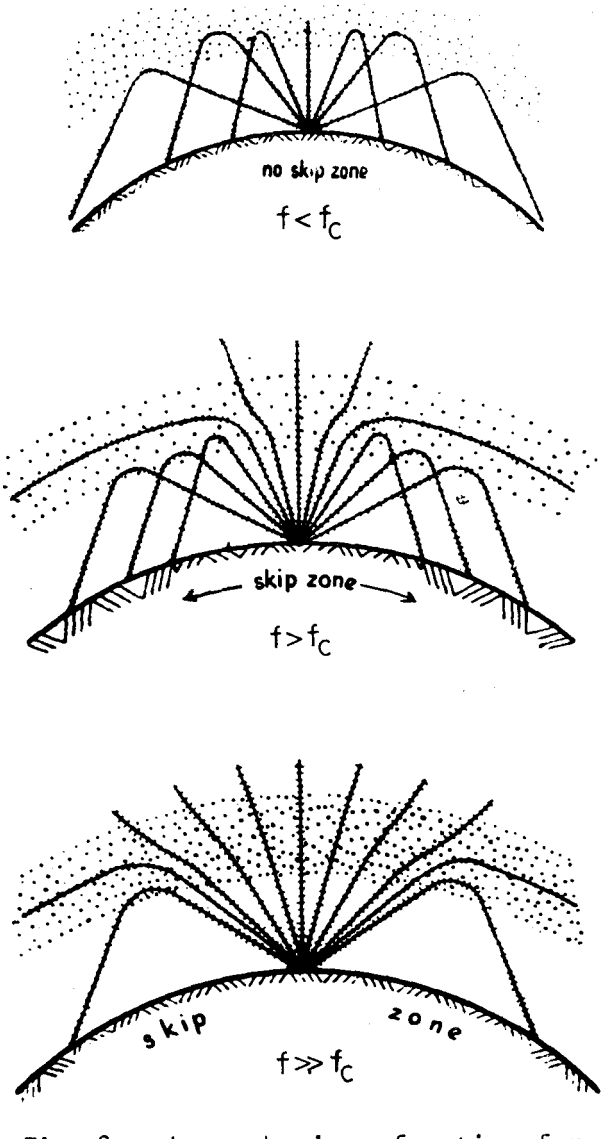

Fig. 2 - Ionospheric refraction for three typical frequencies, increasing from top to bottom[6]

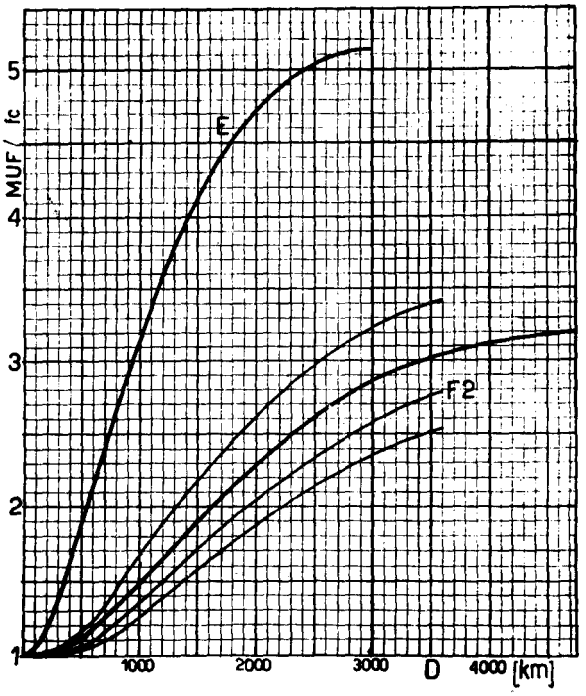

Fig. 3 - 'MUF-factor' (ratio of maximum usable to critical frequency) vs. skip distance (abscissa). Each curve for given height of a thin layer[7]

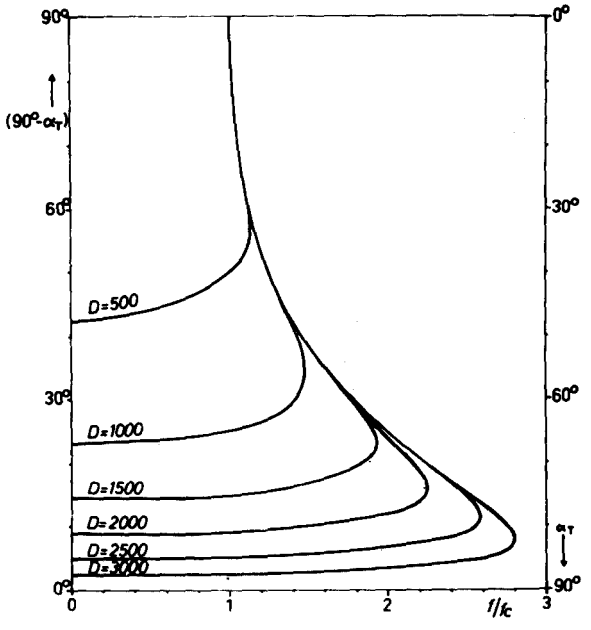

Fig. 4 - Elevation angle for different distances (parameter) depending on frequency ratio f/f_c, parabolic layer, curved Earth and ionosphere[10]

rent altitudes of a thin layer (parameter of the curves)[7]. While echoes from the E-layer have a well defined reflection height, that of the F-region is largely variable, so that several curves were used by the german prediction service during WW II.

2. Early models for Propagation Predictions

In order to take into account the layer thickness, a model of the layer shape had to be assumed. A parabolic shape has often been used to this end. During WW II this model was applied by Maeda[8] in Japan and by Appleton and Beynon[9] in Great Britain. The computation might approximatively take account of the curvature of the ionosphere. For such model Figure 4 shows the computed elevation angle of the transmitted ray of frequency f (abscissa f/f_c) reaching preselected distances D (parameter of the curves). Different from the situation with a layer of negligible thickness, at the high frequency end this angle increases. There also appears a second ('upper') ray to the same distance D, which is called "Pedersen ray". The so-called MUF-factor, f/f_c, is given by the curve enveloping the 'noses' of the individual curves.

Apart from this technique, another solution of the ionospheric propagation problem had been proposed as early as 1937. By combining the geometric relations between angle, height and distance (for a plane ionosphere, but incurved Earth) on the one hand, and the refractive law on the other N. Smith[12] established a set of 'transmission curves', see Fig. 5a. Each curve being valid for a certain frequency one may obtain the virtual reflection height by intersecting the observed ionogram (which gives virtual height as function of frequency at normal incidence). The result of applying the procedure shown in Fig. 5a is reproduced in Fig. 5b. Though this technique was of great interest for scientific studies (e.g. Eyfrig[14]), it was not so much applied for prediction purposes. The high accuracy of the procedure is useless when dealing with medians obtained from a monthly set of largely different individual ionograms.

For propagation purposes, more involved models were later and are still used, e.g. two parabolas (E and F region) with a linear junction[15], or three Elias-Chapmen layers as E, F1 and F2-layers.[16]

3. Empirical Profile Modelling: International Reference Ionosphere

Since early this century, atmospheric profiles of pressure and temperature have been established and were used for different needs. Observations of the first artificial satellites with radio and optical means showed that all models of the upper atmosphere derived up to that time from theoretical reasonings, had largely underestimated the true variations occurring in particular above 100 km of altitude. Therefore, COSPAR established its COSPAR 'International Reference Atmosphere', a set of tables lastly edited in 1972 (Ref. 17). It was then felt that a similar reference should be established for the ionosphere. In 1969, COSPAR and URSI decided to establish a common panel, of which I was chairman until 1984. Having gathered data from different sources, we became aware that, before being taken as a reliable input, some of these needed to be critically discussed. Considering the fast progress of electronic computing, the panel felt that a set of tables might become obsolete soon, and decided to produce a computer program instead. Fears, that this might become a disadvantage for

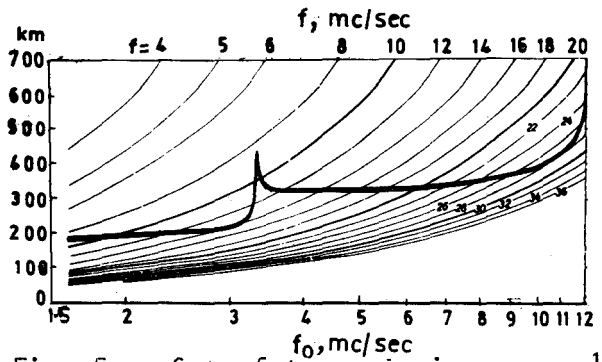

Fig. 5a - Set of transmission curves[12] intersecting the (1st order) ionogram trace (bold). Distance 2000 km[13]

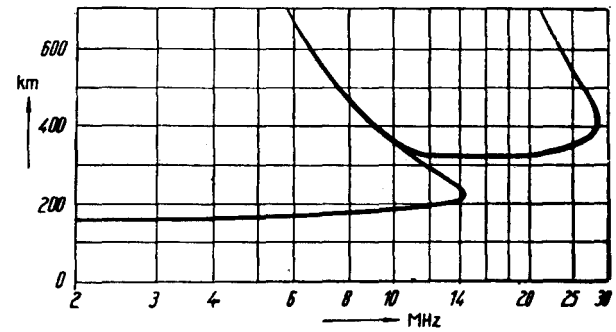

Fig. 5b - Virtual reflection height at oblique incidence obtained from Fig. 5a (Ref 13)

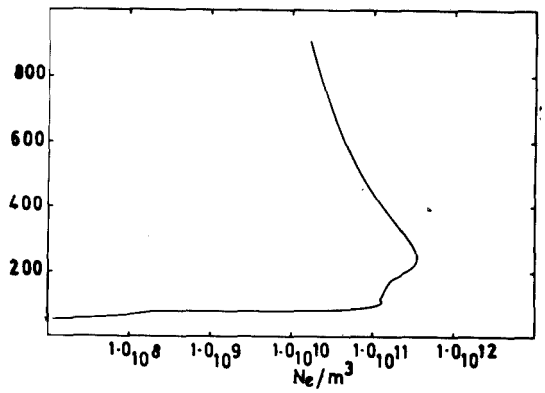

Fig. 7 - Typical electron density profile (day) after IRI

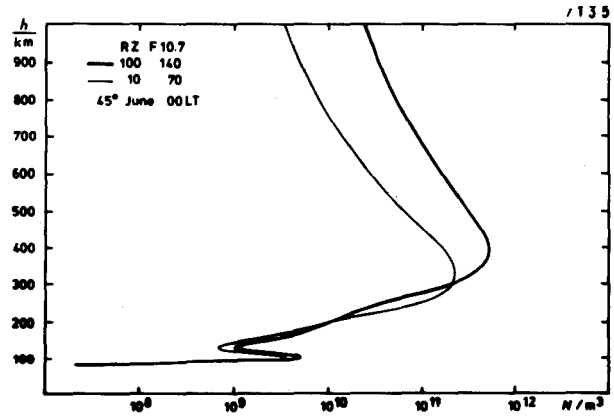

Fig. 8 - Typical electron density profiles (night), after IRI (R = 10, 100)

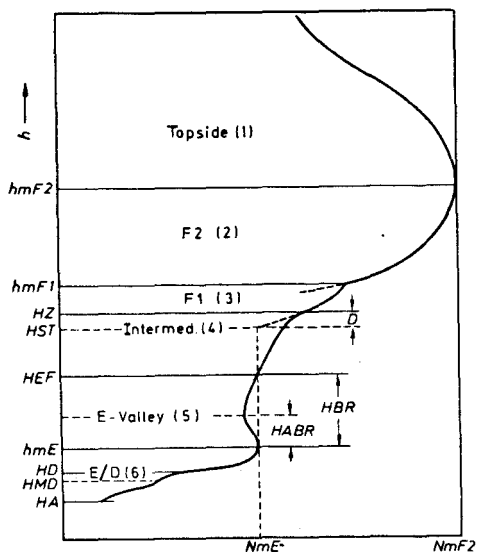

Fig. 6 - Electron density profile, subranges used in IRI-79 (Ref 18)

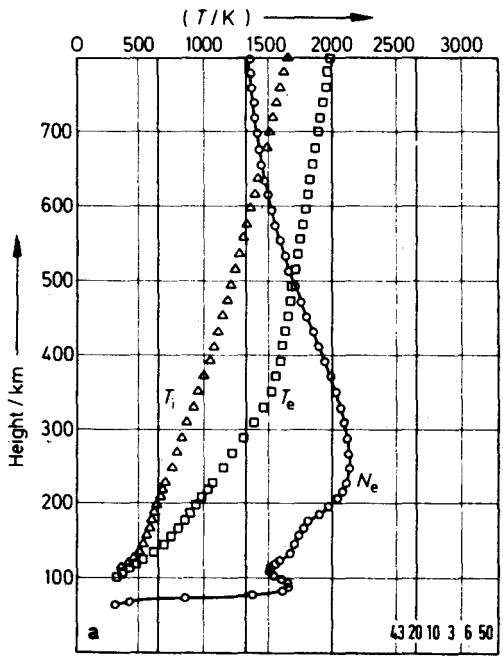

Fig. 9 - IRI density and temperature profiles (43°N, 06 h, March, R = 10)

lated scientists or for those in developing countries, have been dissipated meanwhile. Our first program IRI-78 was first published by URSI in 1978; an improved one describing the state at the end of 1980 (Ref. 18).

Following its terms of reference, IRI allows the computation of height profiles from 70 to 1000 km of the following four parameters of the ionospheric plasma: electron (or positive ion) density, electron and ion temperature, chemical composition (in percent) of positive ions. As a constraint, the parent Unions requested that at lower altitudes both plasma temperature profiles should match the neutral tmeprature profile of CIRA[17]. It was also understood that the peak electron density and the relevant height should be taken from a program[19] established by the competent international agency C.C.I.R. in the International Telecommunication Union (UIT). These so-called 'numerical maps' shall be discussed below.

For the description of electron density, the present IRI uses a height subdivision in several subranges as shown in Fig. 6. The representative functions of the individual subranges are different but continuously connected. This point is now being taken up again; the forthcoming IRI is to apply one fully analytical profile function covering the whole height range[20].

Without discussing details, we present a few examples of IRI electron density profiles in Figs. 7 to 9. Fig.9 shows ion and electron temperature profiles too. An example of an ion composition profile is shown in Fig. 10.

IRI has recently been restructured and partially improved; the new program (tape IRI9) is being distributed right now. This is a preliminary step; a new version of IRI with fully analytic profile description is under discussion[21] and is expected to come out in about two years.

4. Early Aeronomy

The formation of an ionized layer produced by ultraviolet radiation of solar origin falling onto an atmosphere was considered quite early[22-24]. As for the dissipation of ionization, a simple process of direct recombination was assumed; it was described by a recombination coefficient. So, the first approach towards aeronomic theory was production - oriented and assumed local equilibrium of ionization. With this in mind, the multi-layered structure of the electron density profile was difficult to understand. However, after the photo-dissociation of O_2 had been detected[25] it became clear[2] that chemical composition of the upper atmosphere was not homogeneous but changed drastically above an altitude of about 100 km. Figure 11 (also from Mitra's book[5]) shows that this fact was considered as to offer an explanation for the occurrence of several layers, each of these being attributed to the ionization of a particular constituent[26], and/or to a particular range in the solar spectrum[27].

The computation had shown that the intensities given by a black body at 6000 K were by far too small. Therefore, a uv-excess had to be assumed[28].

Systematic differences in the observed ionization had been found for consecutive years. It became soon apparent that the solar cycle of eleven years largely influences the solar radiation power in the extreme

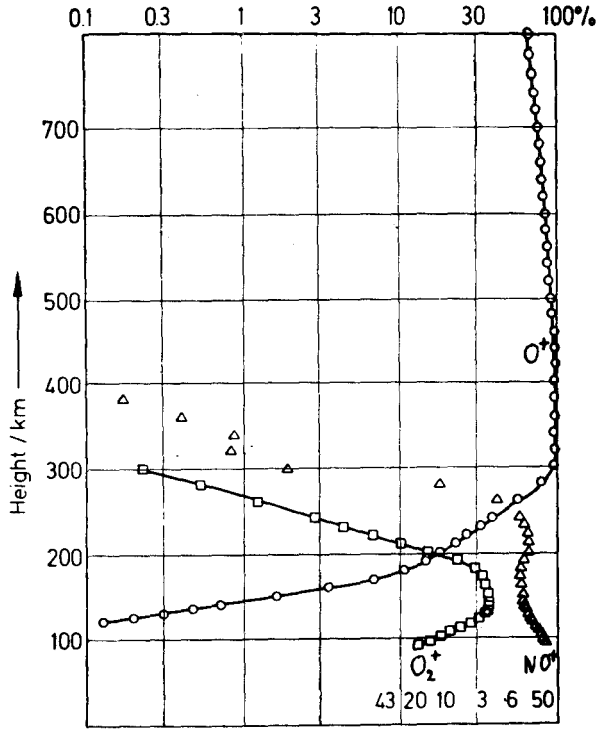

Fig. 10 - IRI composition profiles (O_2 diamonds, NO triangles, O circles)

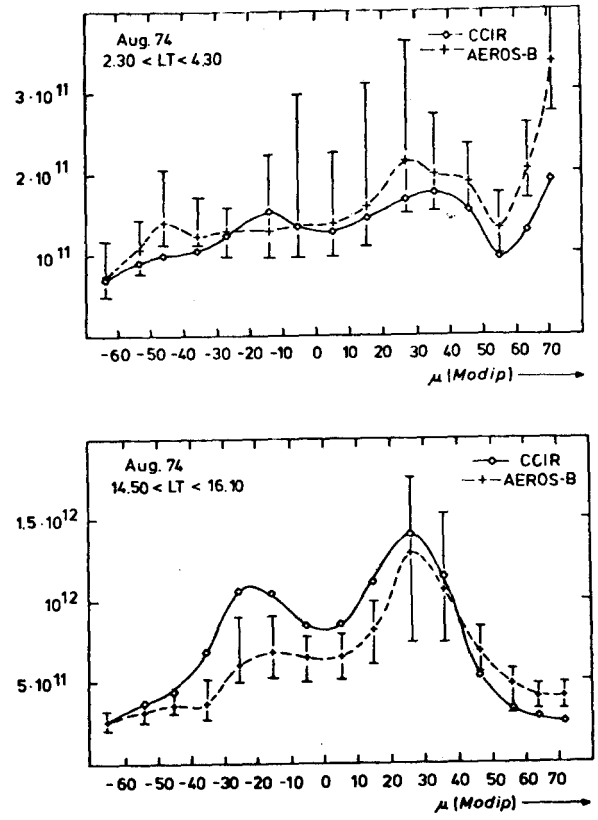

Fig. 14 - Latitudinal cross-sections of peak electron density[45]

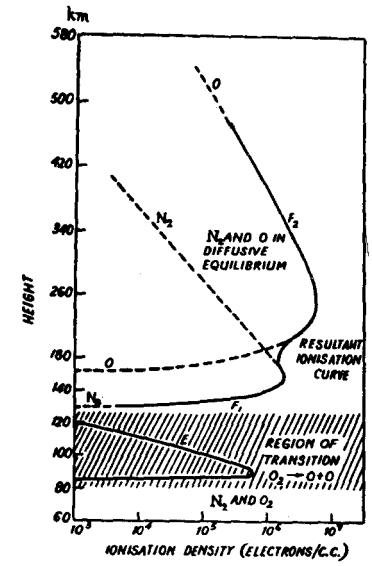

Fig. 11- Production of ionization[5] taking account of dissociation of O_2

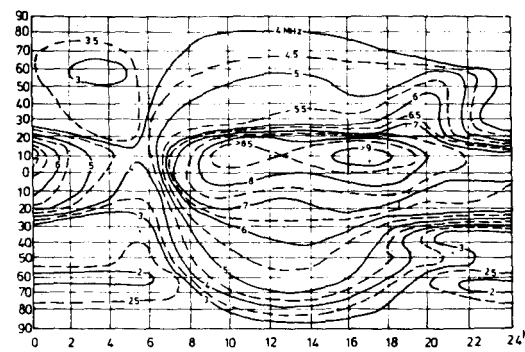

Fig. 12 - Ionization map established in 1944 by German prediction service.

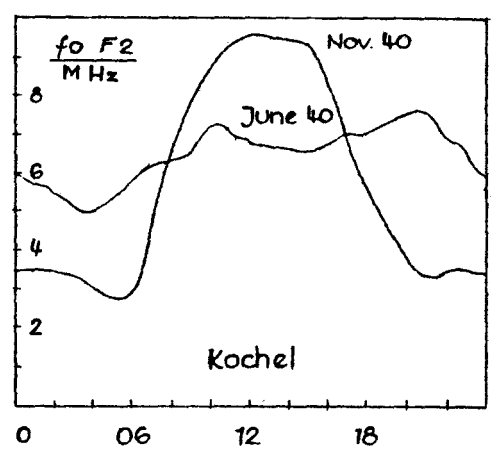

Fig. 13 - Typical monthly average diurnal variation of F2-layer critical frequency (winter and summer)

ultraviolet spectral range. In other words: the excess energy in this spectral range was increased during the 'solar maximum'. The solar activity, then measured by the Zürich sunspot number R_Z, was found to be an important clue influencing the total amount of ionization (see Fig. 8).

Another conclusion was drawn from the assumption of local ionization equilibrium: the highest ionization density should appear at aubsolar latitude. With the then available measurements, peak ionization density maps were established during WW II. It was then felt, that these should peak at that latitude where the solar zenith angle was zero at noon, see Fig. 12.

Though the production-oriented theories gave a first explanation, they were not suited to understand several characteristic features which had been observed. One of these was the so-called summer anomaly, namely the fact that in summer the observed electron density at noon was clearly smaller than in winter (Fig. 13).

Another one was the so-called equatorial anomaly which was first observed during WW II in the pacific ocean[29] and first published by Appleton[30]. Different from the expectations, the observations showed a minimum of ionization at the magnetic equator and maxima to north and south of this latitude, see Fig. 14. So, the F2-layer was under geomagnetic control. The consequence of this was a longitude effect. Geomagnetic (spherical) coordinates were used at first, in order to identify typical longitude ranges. This schedule led to the idea that the pacific and the European-African sectors should be quite similar. However, with the data of a new sounding station at Dakar, it could finally be shown that this was not true[31]. Since that time it is accepted that the real magnetic inclination (or dip) is the decisive element in 'geomagnetic control'.

5. Ion Chemistry

The next step in aeronomy was a more thorough investigation of the dissipation process. One had concluded from quantum-mechanical considerations that the probability should be quite small for direct recombination (in which electron and ion form one neutral atom or molecule). This is a consequence of the large amount of energy set free in the process. So, Bates and Massey[32] forwarded the idea that a process of 'dissociative recombination' should have much higher probability. In such process, a large part of the released ionization energy is taken away by subsequent dissociation of the neutral molecule which must, of course, at least be di-atomic. So, the molecules which at higher levels are more rare than atoms should play an important rôle in the recombination process. At greater heights, this latter is, in fact, a two-stage process: first a charge-transfer reaction from O^+ to an O_2 molecule, then dissociative recombination of the molecular ion with an electron. In addition to recombination each of these processes destroys one O_2 molecule by dissociation. The remaining energy either goes into kinetic energy of the two newly formed atoms or reappears as excitation energy of these latter.

Since that time, ion chemistry has become more and more involved. In general it depends largely on the altitude as a consequence of the changes of the chemical composition of the neutrals and, in particular, the largely different densities. Generally speaking, the complexity of the reactions is greatest at lower heights where collisions are very frequent. It might well be that 20 and more reactions must be considered[33] including a few with excited species[34]. In order to make numerical computations, one needs reaction coefficients, one for each direction of a particular reaction. These are now more and more

often taken from laboratory measurements. Unfortunately, many depend seriously on temperature.

I shall not go into more details but only consider the final result of ion chemistry (see Fig. 15) At a given altitude the production rate by photoionization is computed from the neutral densities, relevant cross-sections and the intensity spectrum of incoming solar radiation. The production rate is the input to a number of loops, one for each ionized species which are coupled by different chemical reactions. In Fig.15 is shown what is globally described as ion chemistry (the large circle). So, the final densities of the different ions are established (small circles).

It is important to note that true equilibrium is only reached in the lower ionosphere. In the F2-layer and above, due to a very low collision frequency, a true equilibrium is never reached because dissipation time constants are larger than the period of daytime photoionization which is about 12 hours.

In the E-region and above, the NO^+ ion is by far more prominent than one should conclude from its primary production rate. This is a consequence of the fact that the relevant ionization energy is somewhat smaller than those of the other species, so that charge transfer away from NO is rather improbable. (Only metallic ions have even lower ionization potential. With their low recombination rate they play an important role in the phenomenon called sporadic E). An example of the typical height variation of the different ion species was shown in Fig. 10.

A particular situation reigns in the lower D-region down to stratospheric heights. Here, molecular ions get to cluster with several neutral molecules, mainly H_2O or CO_2[35,36]. These Cluster ions are much heavier than the molecular ones and have poor stability. Thus, the statistical distribution of the different cluster ions depends largely on temperature. For a reference it was felt that the total percentage of (positive) cluster ions would be a reasonable indication without trying to give a detailed description. Figure 16 which was established by Danilov was accepted as an addendum to IRI[18].

At the same altitudes there might also appear a large number of negative cluster ions such that the total positive ion density can be much larger than the electron density. Since most measurements do only depend on this latter, this phenomenon is the reason for the steep gradient at the bottomside of the D-region. This is quite important for the understanding of vlf-propagation.

6. Plasma Transport

In the F-region and above, plasma cannot freely move since the ions are trapped on magnetic field lines. Collisions are so rare that the free motion of a charge is prescribed as a narrow helix around this line. Therefore, plasma transport by diffusion goes along the field lines. At higher latitudes this may influence the ion density profiles[37], except for the equatorial zone where the field is essentially horizontal. In this context the ions must be regarded as 'leaders' because, by electrostatic force, due to their much larger mass they pull the electrons with them.

If a mechanical force is applied upon the ionospheric plasma, only its component parallel to the magnetic field is able to produce transport. Kohl and King[38] and Stubbe[39] recognized that a drag force exerted by a (horizontal) neutral wind should, therefore, shift the plasma up or down according to the geometry, see Fig.17. So, they were able to explain by wind drag a

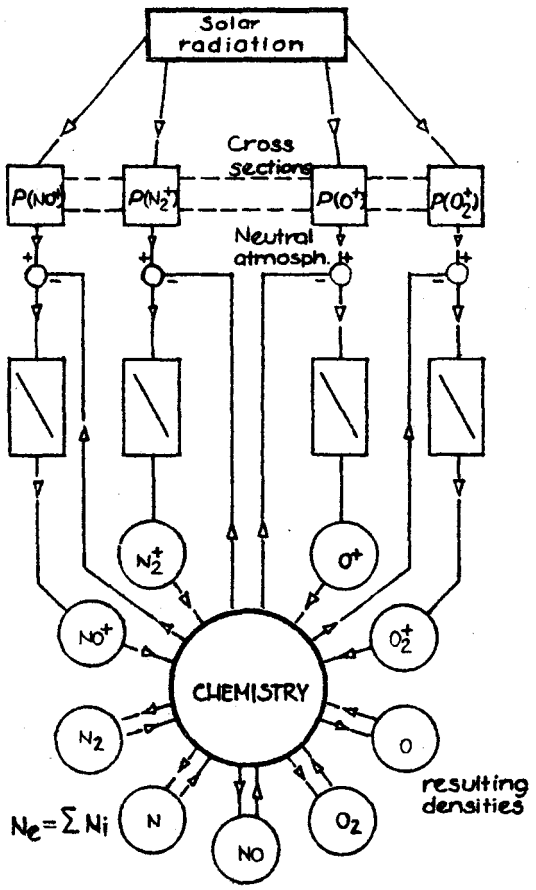

Fig. 15 - Ion chemistry, schematic as an analogue computing system

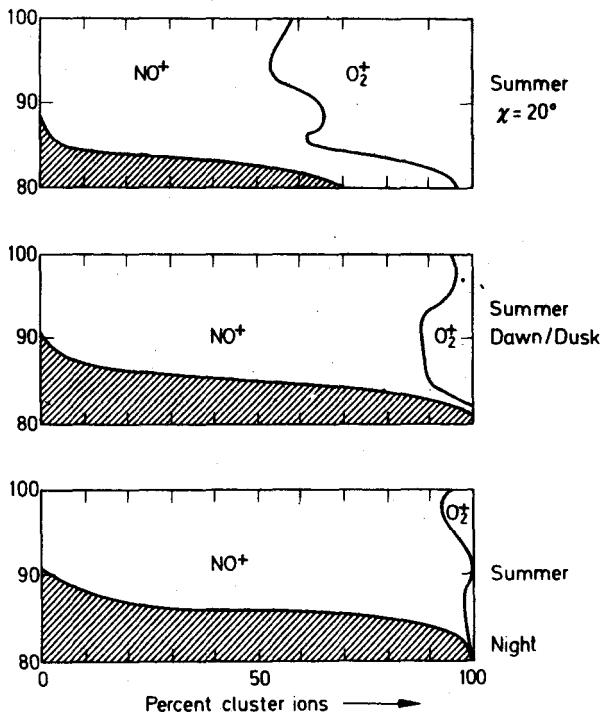

Fig. 16 - Cluster ions, percentage

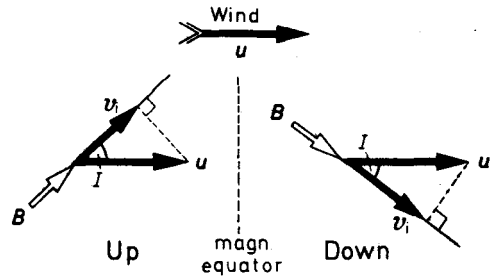

Fig. 17 - Neutral wind drag pushing plasma along field lines

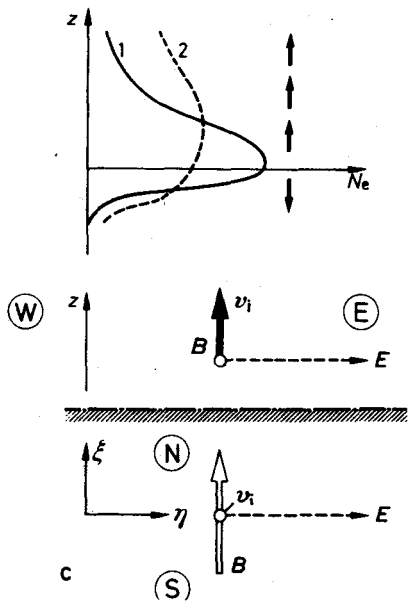

Fig. 18 - El dyn plasma lift near magnetic equator ('fountain').

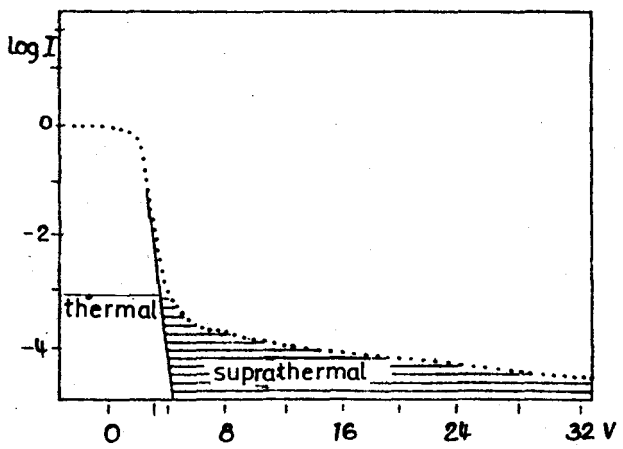

Fig. 21 - Electron energy spectrum measured by Spenner on AEROS-B[46]

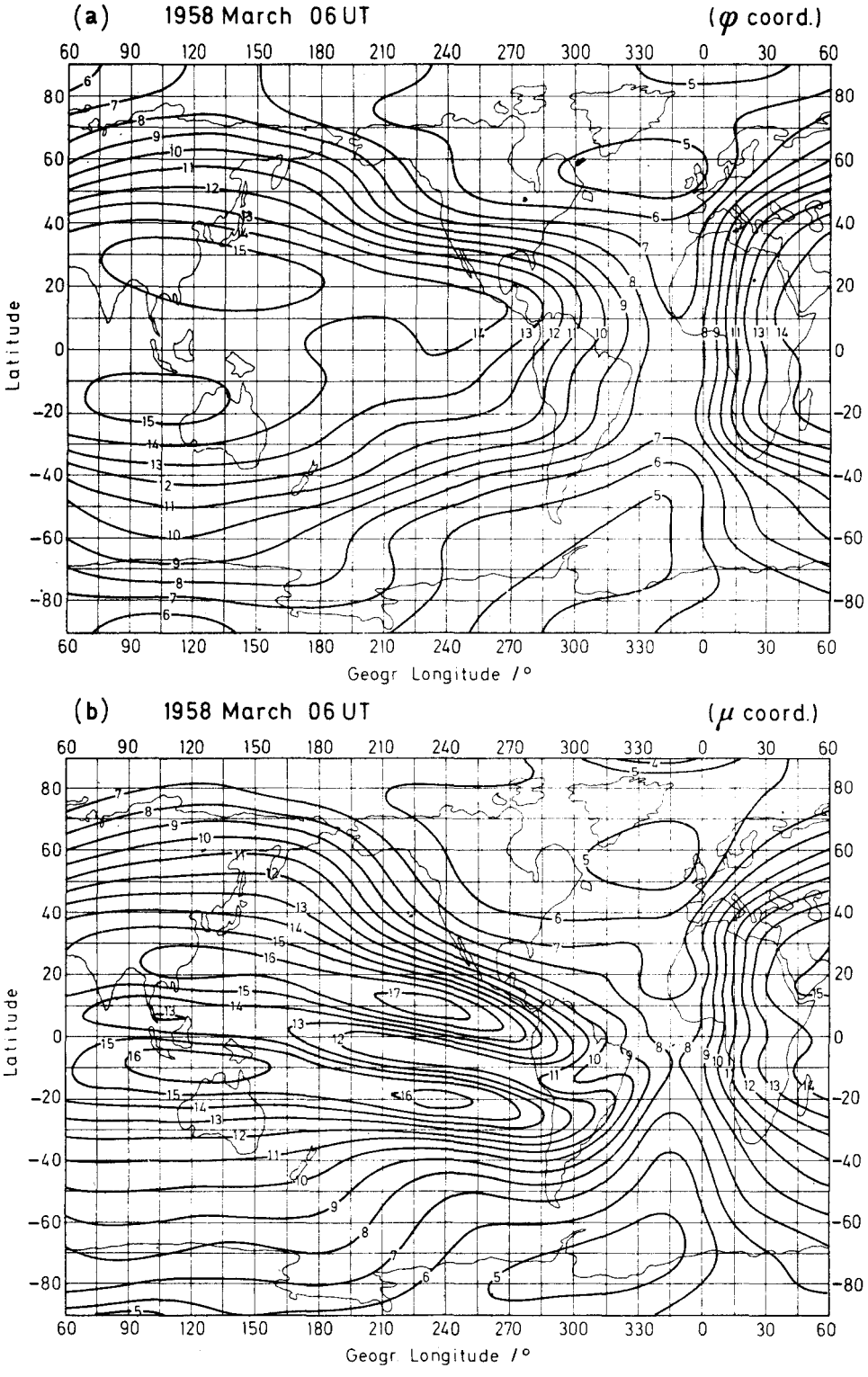

Fig. 19 - Ionization maps by the Gallet-Jones method for March 1958, 06 h UT, using (a) geodetic, (b) modified dip as latitude for shifting screen stations /Courtesy: C Rush/.

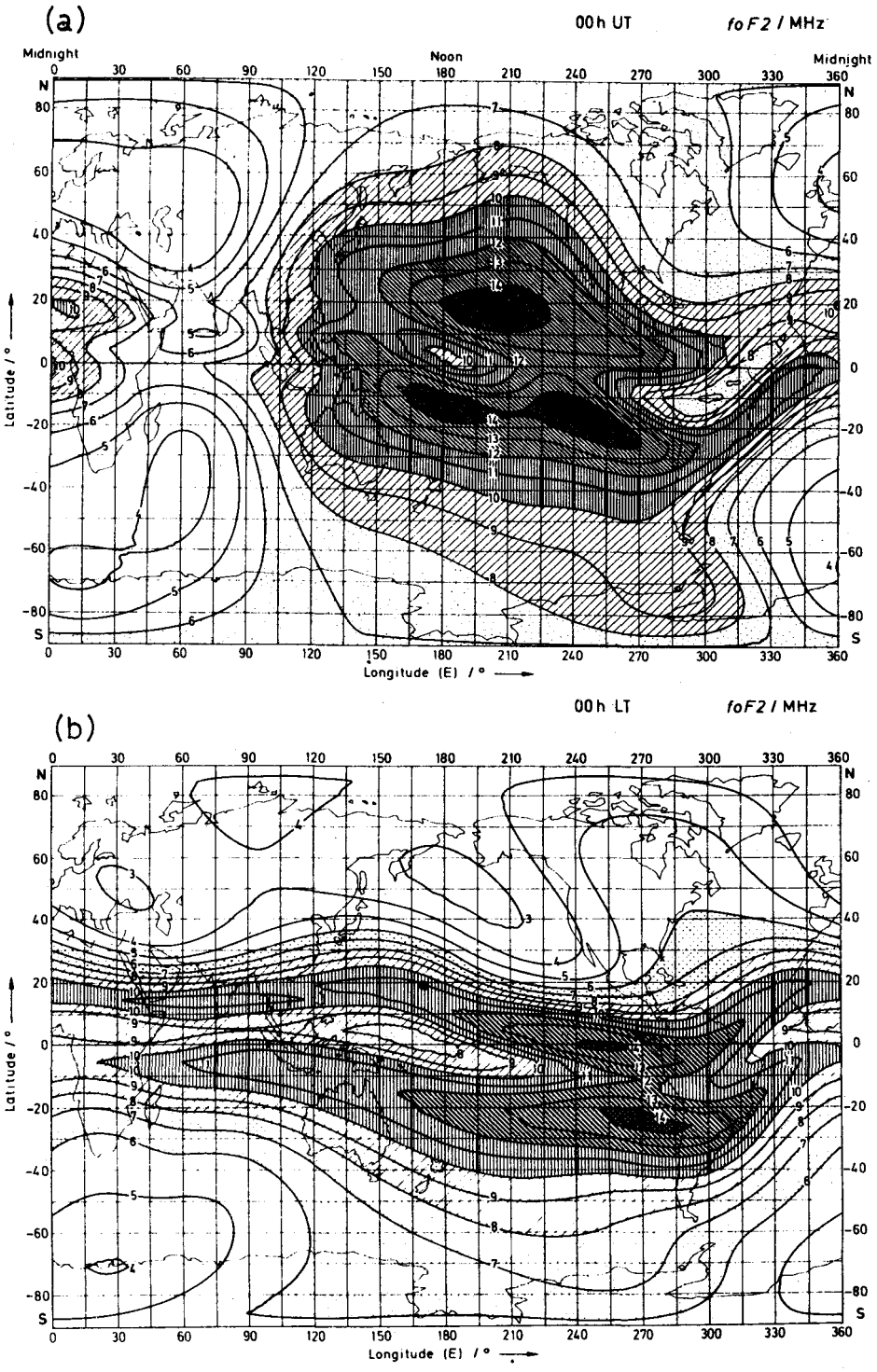

Fig. 20 - Ioniszation maps established from japanese satellite observations[44].
(a) for 00 h UT,
(b) for 00 h Local Mean Time.

large part of the sometimes queer diurnal variations, in particular the 'summer anomaly' (see Fig. 13). Of course, near the dip equator wind drag cannot change the plasma density profile because only horizontal motion could be provoked which does not change the profile.

There exists, however, a force that moves the ions perpendicularly to the magnetic lines of force. It is electromagnetic in nature and proportional to $\underline{E} \times \underline{B}$, thus always perpendicular to the magnetic field line, $\underline{B}$. So, any electric field which is not parallel with $\underline{B}$, moves the plasma across the magnetic field lines. This is very important near the dip equator where, by day, the magnetic field is horizontal in NS direction, and the equatorial electrojet is driven by a horizontal electric field in EW-direction. Thus, an electromegnetic (Lorentz-) force is exerted upon the plasma lifting it upwards by a few hundered kilometres, according to the strength of the fields. Once arrived at the peak, the motion stops and the gravity force drives the plasma down again now, of course, along the magnetic field line[40,41]. This 'electromagnetic fountain' (Fig. 18) explains why, by day, the electron density is decreased at the magnetic (dip) equator and increased north and south of this latter. This is the explanation of the equatorial anomaly (see Fig.14)

7. Worldwide mapping

As explained above (see end of Section 4) and shown by Fig. 14, the relative ion density minimum at the true magnetic equator was empirically known long before its theoretical explanation was found. Long before its detection, worldwide maps of the F2-layer critical frequency foF2 were established for propagational purposes, see Figs. 12 and 14. (Note that the square of this critical frequency is proportional to the peak plasma density). Such maps, giving foF2 as function of latitude and local hour were originally drawn by hand after plotting the (monthly average) data of each station at its latitude (ordinate).

Gallet was first in trying to computerize mapping, taking account of longitude too. Due to the very inhomogeneous distribution of the ionospheric sounding stations, trials to reproduce directly the observed data did not succeed. Then, Jones and Gallet[42] introduced a scheme which is still applied: they started with the monthly mean diurnal variation which was first Fourier-analyzed to the 7th order. So, 15 Fourier-coefficients were found for each station. Now, each of these coefficients is worldwide developed using the well-known set of Legendre-functions (also called 'associated spherical functions'). So, with a large number of coefficients, a world-wide functional description is reached. In order to find the value of foF2 at any given site, the method is applied in the inverse direction: from each of the 15 sets of Legendre-developments the value of the relevant Fourier-coefficient is found. The foF2 diurnal curve is then produced by Fourier-synthesis.

This scheme did not everywhere give reasonable results, in particular in oceanic areas. In order to improve it, Jones and Gallet[42] introduced 'virtual stations', just by shifting continental stations into the oceans onto positions of equal latitude. These 'screen stations' are given the same Fourier-data as had been found at the original station. Figure 19a is an example of a map obtained with this procedure.

However, the result was not in agreement with geomagnetic control: the characteristic behaviour around the dip equator (see Fig. 14) was wiped out. Therefore, when the subject was dealt with in the Comité Consultatif International des Radiocommunications (C.C.I.R.), W G Baker checked different systems of coordinates and finally came down with the

so-called 'modified dip' latitude, originally proposed by Rawer[43]. Figure 19 shows that magnetic dip control is safeguarded when this coordinate is used at the shifting of real stations onto 'screen' positions. With this change the Gallet and Jones method was finally accepted by C.C.I.R. and remained the official 'numerical map' until to-day[19].

Direct evidence about the true behaviour above the oceans could only be obtained from satellites, provided their on-board memory had enough capacity to store the measured data until the next ground telemetry stations could be contacted. The early top-side-sounding satellites did not allow for this to be done. Recently, however, the Japanese ISS-b satellite was able to produce enough data so as to apply the Legendre analysis as used by C.C.I.R. Unfortunately, data of four consecutive months were in fact needed to this end; thus, the results are yet influenced by some seasonal variations. Figures 20a, b[44] are examples. Figure 20a is a 'snap shot' of the world at a given hour UT; therefore, the longitudinal variation seen on this map is mainly due to that of the local hour. The true longitudinal effect appears from Fig. 20b which is for a given (night time) local hour.

In situ measurements of satellites have also shown that the longitude effect is larger above the oceans[45] than seen from the C.C.I.R. numerical maps. This results from the fact that minimum and maximum of the longitudinal variation happens to be found above the oceans.

Thus, the numerical mapping problem needs being rediscussed. At its 1984 General Assembly, URSI has set up a new panel on this subject.

8. Heating effects

For computations of the ion chemistry (see Section 6) all relevant coefficients must be numerically known. Unfortunately, these undergo large variations with temperature. Therefore, aeronomic computations cannot avoid taking account of temperature.

Solar radiation is the principal heating source in the upper atmosphere. However, it does not equally heat up all constituents. The main heat input occurs in conjunction with photoionization , the energy set free being almost entirely taken by the photo-electron. This photoelectron population has energies around 10 eV which is large against thermal energies. Of course, collisions with the thermal electrons provoke a degradation so that finally a continuous energy spectrum is found (Fig. 21); the largest number of electrons remain thermal but with an increased temperature. Because the collisional heat contact with the heavier ions is much weaker, these are only slowly heated up and so are the neutrals. In the F-region the time constants of these processes are longer than the daily sunshine period so that equilibrium is never reached. Therefore, by day the temperatures of the different species are different:

$$T_{e\,ph} > T_e > T_i \gtrsim T_n$$

(Indices identify photoelectrons, electrons, ions and neutrals). The lack of temperature equilibrium is a characteristic feature of the dayside upper atmosphere.

Typical electron and ion temperature profiles, as given in IRI, were shown in Fig. 9. Figures 22 show IRI compared with incoherent scatter measurements from Jicamarca (at the magnetic dip equator) and Arecibo (30^{o} N geomagn) and with AEROS satellite measurements. These low latitude stations show a monotonuously increasing ion temperature (Fig. 22a). The electron temperature, however, shows one maximum at about 200 km, followed by a minimum and a new increase to even higher values. At middle latitu-

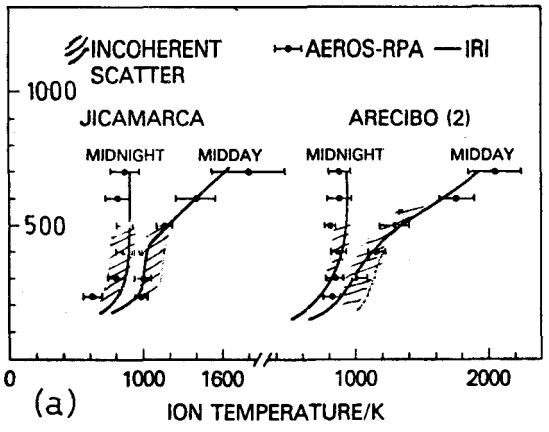

Fig. 22a - Ion temperature profiles obtained by incoherent scatter (hatched) and by satellite AEROS-B (bars) [46]. Curves IRI-79.
Left Jicamarca (Peru, dip equator), right Arecibo (Puerto Rico)

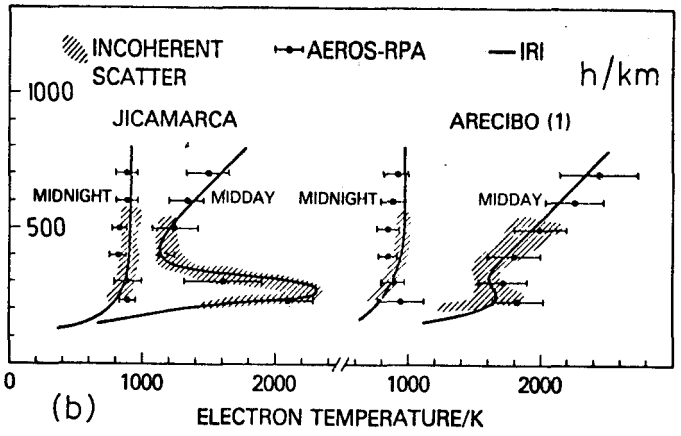

Fig. 22b - Electron temperature profiles obtained by incoherent scatter (hatched) and by satellite AEROS-B (bars) [46]. Curves IRI-79.
Left Jicamarca (Peru, dip equator), right Arecibo (Puerto Rico)

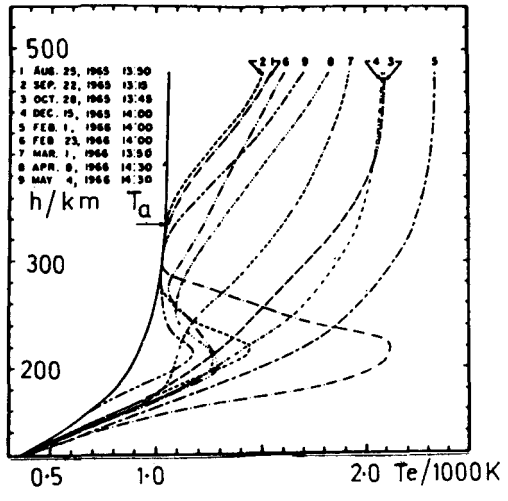

Fig. 23 - Typical electron temperature profiles measured at noon by incoherent scatter at Arecibo (Puerto Rico). Curves in order: 1965: 25 Aug, 22 Sep, 28 Oct, 15 Dec. 1966: 1 Feb, 23 Feb, 1 Mar, 8 Apr, 4 May.
/Courtesy: J V Evans/

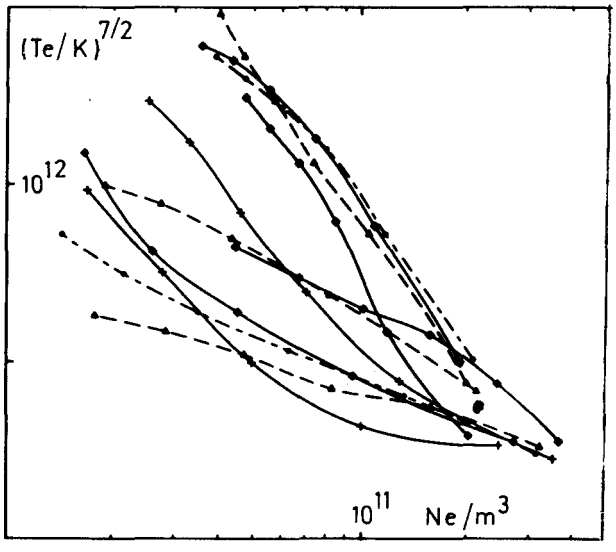

Fig. 24 - Electron temperature (to power 7/2, ordinate) vs. electron density (abscissa). Monthly median relations (of a few days only), different months.
/Courtesy: D Bilitza/

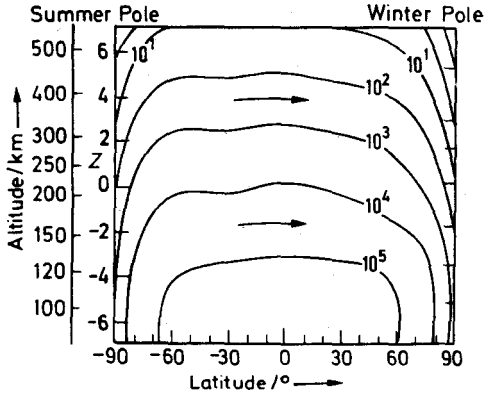

Fig. 25 a - Global wind system mainly due to solar heat input /after Roble/. Arrows indicate transport towards winter pole. Curves: total flux/kg.s^{-1} (above given height, ordinate). Abscissa: latitude.

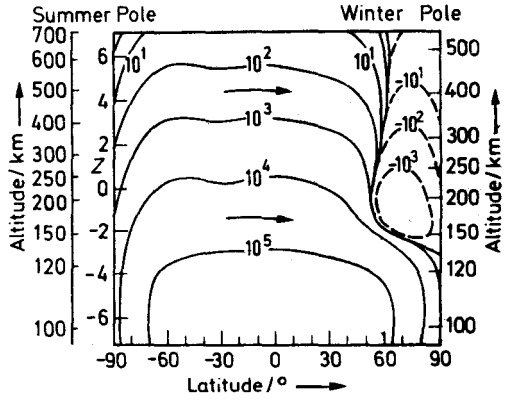

Fig. 25 b - Global wind system when solar and corpuscular heating are both important (the latter in the polar caps, see Fig. 26). Around the winter pole, in the thermosphere, an extra cell appears.

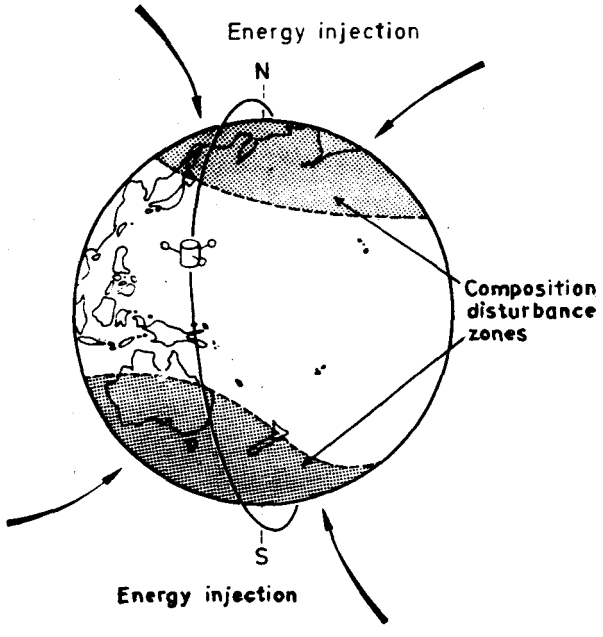

Fig. 26 - Corpuscular heating of the polar caps by particle flux arriving from the magnetospheric tail

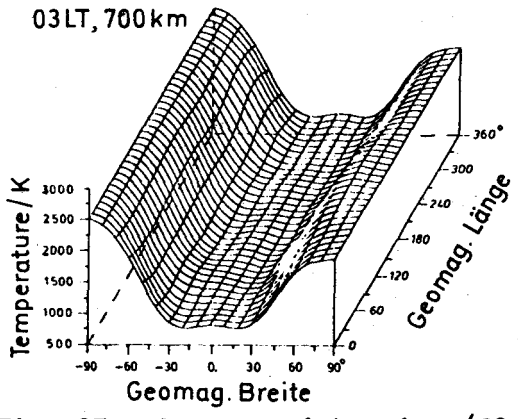

Fig. 27 - Average night time (03 h local time) electron temperature as observed by Spenner aboard satellite AEROS-A[46] depending on geomagnetic latitude (abscissa) and longitude (depth). Altitude: 700 km

ACKNOWLEDGEMENT

Figures 2, 3 and 5 were taken from: K Rawer, Die Ionosphäre, Groningen 1953 with kind permission of P Noordhoff N.V. Figures 10, 17, 18, 19, 20, 22, 25 and 26 were taken from K Rawer's contribution in: Handbuch der Physik (Encyclopedia of Physics), Vol. 49/7, Berlin 1984 with kind permission of Springer-Verlag.

des, the solar heating effect is smeared out over a large height range by diffusion along the lines of force. At low magnetic latitudes, however, vertical heat transport could only be brought about by electric fields (see Section 6). As for the temperature increase towards exospheric heights, there exists a second heat source due to collisions with electrons trapped on the closed fieldlines in the inner magnetosphere.

The thermospheric maximum at low latitudes is, of course, quite important at the magnetic equator (Jicamarca, left hand side in Fig. 22b). Arecibo (right hand side) shows a much smaller average maximum. It was, however, found that there exist appreciable differences between different months as shown by Fig. 23. This seasonal variation (due to the seasonally variable solar zenith angle) is not yet taken account of by IRI.

Since the heat conductivity in the electron gas, as well as heat transfer to ions and electrons increase drastically with the plasma density, N_e, one should expect a decrease of the electron temperature, T_e. This is in fact observed. Figure 24 presents monthly graphs of T_e vs N_e. All of them show the expected relation but not all with the same shape (Power 7/2 of T_e was plotted in Fig. 24 in order to check an early theory predicting a linear relation with N_e).

9. Modelling

Since transport and heating have been found to be first order influences in aeronomy on the spot computations cannot yield a satisfying solution. Therefore, global transport has been modelled, at first for understanding neutral atmosphere changes. Roble found out that at higher altitude mass flow should , by day, mainly go from the summer pole towards the winter pole (Fig. 25a). However, looking deeper into observed neutral transport, he found that this was not always true. In most cases, there exists a quite appreciable third heat source which is due to corpuscles travelling with high speed along the open field lines of the magnetospheric tail and so reaching the polar cap (Fig. 26). Unfortunately, this heat source is so largely variable that Roble did not feel worthwhile to consider an average situation. Instead he decided to make the computations for individual days for which some measurements related to the actual heat input were available (preferentially electron temperature at high latitude and altitude).

This kind of modelling gave results which compared well with observed data. As a result of polar cap heating, the simple picture of Fig. 25a could no more be upheld. A new circulation cell was found at high latitude, the size of which depends largely on the importance of the heating, see Fig. 25b.

The average importance of polar cap heating can be clearly seen from global electron temperature data. Figure 27 shows the average nighttime T_e at 700 km, as observed by the AEROS-A satellite[46]. There is a clear increase at high latitudes.

Another modern effort goes towards modelling the polar cap conditions themselves. Computer simulation is helpful in this context. The computations, made by Schunk and Sojka[47], are very promizing though needing a very large amount of computing time.

References

1. Stewart B, Ency Brit (9°), 36 (1882).

2. Schuster A, Phil Trans Roy Soc (London) A 180, 467 (1889) & 208, 163 (1908)

3. Kennely A E, Elect World & Eng 15, 473 (1902).

4. Heaviside O, Ency Brit 16, 181 (1902).

5. Mitra S K, The Upper Atmosphere (The Royal Society of Bengal, Calcutta), 1948.

6. Rawer K, Die Ionosphäre (Nordhoff, Groningen), 1952; The Ionosphere (Ungar, New York), 1957.

7. Dieminger W in Bartels J (editor), FIAT Review of German Science 1939-1946 (Dietrich'sche Verl Buchh, Wiesbaden), I, 17, 93-163 (1948).

8. Maeda K-I & Kohno T, Nippon Elect Commun Engng 236 (1940).

9. Appleton E V & Beynon W J G, Proc Phys Soc (London) 59, 58 (1947).

10. Rawer K, Revue Scientif 86, 585 (1948).

11. Pedersen P O, The Propagation of Radio Waves (Danmarks Naturwidenskabelige Samfund, Copenhagen), 1927.

12. Smith N, Nat Bur Stand J Res 19, 89 (1937) & Proc IRE, 27,332 (1939).

13. Rawer K, The historical development of forecasting methods for ionospheric propagation of HF waves, Radio Sci 10, 669-679 (1975).

14. Eyfrig R, Hochfrequenztechnik u El Ak 56, 161 (1940).

15. Bradley P A & Dudeney J R, J Atmos Terr Phys 35, 2131 (1973).

16. Chiu Y T, J Atmos Terr Phys 37, 1563 (1975).

17. Commitee on Space Res, CIRA 1972, COSPAR international Reference Atmosphere (Akademie Verlag, Berlin), 1972.

18. Rawer K (chmn), Lincoln J V & Conkright R O (eds), International Reference Ionosphere - IRI-79, Rep UAG-82, World Data Center-A for Solar-Terrestrial Physics, Boulder,Co, USA, 1981.

19. Comité Consultatif International des Radiocommunications (CCIR), CCIR Atlas of Ionospheric Characteristics, Rep 340 (UIT, Genève) 1967/1983.

20. Rawer K, Adv Space Res 4 (1), 11 (1984).

21. Rawer K & Minnis C M (editors), Adv Space Res 4 (1), 1984 & 5 (7) 1985.

22. Lenard P, Über die Absorption der Nordlichtstrahlen in der Erdatmosphäre, Sitzungsber. Heidelberger Akad d Wiss, 1911 /apparently first to consider the hit count for a stream of corpuscles/.

23. Elias G J, Tydschr Ned Radio Gen 2, 1 (1923).

24. Chapman S, Proc Phys Soc 43, 26 & 483 (1931).

25. Majumdar R C, Ind J Phys 12, 75 (1938).

26. Bhar J N, Ind J Phys 12 363 (1938).

27. Nicolet M, Contribution à l'étude de la structure de l'ionosphère, Mém 19, Inst Royal Météo Belgique, 1945; Schröer E, ZS f Meteorologie 1, 110 (1947).

28. Kiepenheuer K O in Ten Bruggencate P (editor), FIAT Review of German Science 1939-1946 (Dieterich'sche Verl Buchh, Wiesbaden), I. 10, 228 1948.

29. First detected by Maeda K-I (Japan), then by Smith N, Lindemann-Philips M & Bailey D K (USA) and by Eckersley T L (GB) /private communication by Gillmor C S 1985/.

30. Appleton E V, Nature (London) 157, 691 (1946).

31. Oboril F & Rawer K, CR Paris 228, 1962 (1949).

32. Bates D R & Massey H S W, Proc Roy Soc (London) 192, 1 (1947).

33. Torr D G, Rev Geophys Space Phys 17, 510 (1979).

34. Torr M R & Torr D G, Rev Geophys Space Phys 20, 91 (1982).

35. Arnold F, in [18], 19 (1981).

36. Kopp E, in Rawer K & Minnis C (editors), Experience with and Proposed Improvements of the International Reference Ionosphere, Center-A for Solar-Terrestrial Physics, Boulder,Co, USA, 140, 1984.

37. Yonezawa T, in Rawer K (editor), Handbuch der Physik XLIX/ 6, 129-245, 1982.

38. Kohl H & King J W, Nature (London) 206, 699 (1965); Rishbeth H Megill L R & Cahn J H, Ann Geophys 21, 235 (1965).

39. Stubbe P in Rawer K (editor), Handbuch der Physik XLIX/6, 247-308, 198

40. Rishbeth H Lyon A J & Peart M J, J Geophys Res 68, 2559 (1963).

41. Bramley E N & Peart M J, J Geophys Res 69, 4609 (1964).

42. Jones W B & Gallet R M, Telecomm J 29, 129 (1962) & 32, 18 (1965).

43. Rawer K , in Landmark K B (editor), Meteorological and Astronomical Influences on Radio Wave Propagation (Academic Press, New York), 221, 1963.

44. Matuura N, Atlas of Ionospheric Critical Frequencies (foF2) from Ionosphere Sounding Satellite-b Observations, Rep Radio Res Labs, Tokyo, 1979.

45. Sheikh N M Neske.E Rawer K & Rebstock C, Telecomm J 45, 225 (1978).

46. Lämmerzahl P Rawer K & Roemer M, Ergebnisse des AEROS-Satellitenprogramms, Rep MPI H-1980-V3, MPI Kernphysik, Heidelberg, 1979.

47. Schunk R W & Sojka J J, J Geophys Res 87, 5169 (1982) & 89, 2348 (1984).